

Centennial-scale intensification of wet and dry extremes in North America

Kyungmin Sung¹, Gil Bohrer², and James Howard Stagge¹

¹The Ohio State University

²Ohio State University

April 30, 2023

Abstract

Drought and pluvial extremes are defined as deviations from typical climatology; however, the background climatology can shift over time in a non-stationary climate, impacting interpretations of extremes. This study evaluated changes in meteorological drought and pluvial extremes by merging tree-ring reconstructions, observations, and climate-model simulations spanning 850 – 2100 CE across North America to determine whether the Industrial era and projected future lie outside the range of natural climate variability. Our results found widespread and spatially consistent exacerbation of both extremes, especially summer drought and winter pluvials, with west and south drying, the northeast wetting trends, and increased interannual variability across the east and north. Our study underscores climate change has already shifted precipitation climatology beyond pre-Industrial climatology and is projected to further intensify ongoing shifts.

Hosted file

960961_0_art_file_10920754_rth150.docx available at <https://authorea.com/users/610919/articles/639697-centennial-scale-intensification-of-wet-and-dry-extremes-in-north-america>

Hosted file

960961_0_supp_10889350_rt0t2b.docx available at <https://authorea.com/users/610919/articles/639697-centennial-scale-intensification-of-wet-and-dry-extremes-in-north-america>

1
2
3
4
5
6
7
8
9
10
11
12
13
14

Centennial-scale intensification of wet and dry extremes in North America

Kyungmin Sung¹, Gil Bohrer¹, James Stagge¹

¹Civil, Environmental and Geodetics Engineering, The Ohio State University, Columbus, Ohio

Corresponding author: James Stagge (stagge.11@osu.edu)

Key Points:

- This study models seasonal drought and pluvial trends, merging reconstructions, observations, and projected from 850 to 2100 CE.
- Results show widespread exacerbation of both extremes with overall drying (wetting) in the southern (northeastern) North America.
- Modern drought and pluvial distributions are outside pre-Industrial (1850) conditions, and exhibiting substantial shifts in some regions.

15 **Abstract**

16 Drought and pluvial extremes are defined as deviations from typical climatology; however, the
17 background climatology can shift over time in a non-stationary climate, impacting interpretations
18 of extremes. This study evaluated changes in meteorological drought and pluvial extremes by
19 merging tree-ring reconstructions, observations, and climate-model simulations spanning 850 –
20 2100 CE across North America to determine whether the Industrial era and projected future lie
21 outside the range of natural climate variability. Our results found widespread and spatially
22 consistent exacerbation of both extremes, especially summer drought and winter pluvials, with
23 west and south drying, the northeast wetting trends, and increased interannual variability across
24 the east and north. Our study underscores climate change has already shifted precipitation
25 climatology beyond pre-Industrial climatology and is projected to further intensify ongoing
26 shifts.

27 **Plain Language Summary**

28
29 Managing water resources has become challenging due to effect of human-caused climate
30 change on extremes. This study examines trends in droughts and pluvials (extreme wet periods)
31 from the distant past (850 CE) to the projected future (2100 CE) to determine whether
32 precipitation extremes in the modern, Industrial era and the future are beyond what is typical of
33 natural climate variability in North America. Gradual precipitation trends were generated by
34 merging information from tree rings, observations, and climate models using a novel statistical
35 approach to correct bias. Results indicate the widespread intensification of both drought and
36 pluvials – especially summer drought and winter pluvials during the modern and future periods.
37 Spatially, southern and western regions are becoming drier, while the northeast is getting wetter,
38 and intermediate regions show a wider range between drought and pluvial years. Our study
39 suggests that anthropogenic climate change has already modified drought and pluvial extremes
40 beyond natural, pre-Industrial conditions and these ongoing trends are projected to intensify
41 through the future. Wider ranges between extreme dry and wet years increases risk for water
42 management and shows the need for adapting water strategies to account for the "new normal" of
43 the climate change.

44 **1. Introduction**

45 Quantifying precipitation non-stationarity is particularly important given the impact of
46 anthropogenic climate change overlaid onto longer patterns of natural climate variability (Stahle
47 et al., 2020; Williams et al., 2022). Future hydroclimate projections indicate intensifying
48 extremes, such as droughts or pluvials (periods with sustained high precipitation) for many
49 regions, shifting what was historically extreme to become more commonplace (Ault, 2020;
50 Bishop et al., 2021; Stevenson et al., 2022). This has critical implications for water management
51 systems and policies designed using early 20th century climate baselines, which may no longer be
52 representative of current or future hydroclimate, increasing risk and vulnerability.

53

54 Some regions have already experienced such changes. Mean annual precipitation in the eastern
55 US has generally increased over the past century, while that of western US has decreased, with
56 those changes during the past 100 years likely the most rapid since 1400CE (B. Cook et al.,
57 2019; Williams et al., 2022). These trends are attributed to anthropogenic global warming
58 combined with complex natural variability (Diffenbaugh et al., 2015, 2017; Hoylman et al.,
59 2022; Lehner et al., 2017), which can be better understood when placed in the context of
60 centuries of pre-Industrial natural variability.

61

62 This study merges tree-ring proxy reconstructions, gridded observations, and Global Climate
63 Model (GCM) output to quantify climate non-stationarity at a centennial-scale, permitting an
64 estimation of anthropogenic climate change impacts on drought and pluvials relative to natural
65 pre-Industrial variability. Modern observations often extend a century into the past, while tree-
66 ring reconstructions can extend more than 1000 years (Bishop et al., 2021), and GCMs can
67 simulate climate over centuries from the distant past through feasible future emissions scenarios
68 (Marvel et al., 2021). Merging these datasets creates challenges due to unique biases, stemming
69 from tree growth sensitivities in reconstructions and systematic model biases in GCMs (Cui et
70 al., 2021). Additionally, temporal and spatial resolution differences complicate the creation of a
71 merged series. For example, the North American Seasonal Precipitation Atlas (NASPA) proxy
72 reconstruction used here provides bi-annual precipitation estimates, comprised of one 5-month
73 cool season and one 3-month warm season (Stahle et al., 2020); far coarser than daily or
74 monthly resolution of the other datasets.

75 Hence, this study aims to address: (1) whether future projections of wet and dry precipitation
 76 extremes are significantly different from the past 1000 years, and (2) how trends during the
 77 instrumental period (1900 – 2020CE) fit into the longer pattern of natural climate variability and
 78 anthropogenic climate change. This is accomplished through a novel non-linear spline model
 79 (Stagge & Sung, 2022; Sung et al., 2022) which simultaneously corrects data-induced bias to
 80 generate a single, common model of century-scale shifts in the 3-month Standardized
 81 Precipitation Index (SPI-3) (Heim, 2002), representing drought and pluvial extremes.

82 2. Methods

83 2.1. Data

84 Precipitation estimates were based on tree-ring reconstructions (NASPA), processed gridded
 85 observations (CRU and GridMET), and two CMIP6 model simulations (MRI-ESM2-0 and
 86 MIROC-ES2L, Table 1) . Two CMIP6 models were chosen because they provide simulations of
 87 the full period 850-2100 CE via the *past1000* (850 to 1849 CE), *historical* (1850 to 2014 CE),
 88 and *ScenarioMIP* experiments (2015-2100 CE). We considered two future Socioeconomic
 89 Shared Pathways (SSPs) to bracket potential futures from the “business as usual” high emissions
 90 scenario, SSP 5-8.5, to the low emissions scenario, SSP1-2.6 (Eyring et al., 2016).

91 Table 1. Datasets.

Name	Model	CMIP6 Experiment	Period	Spatial Resolution
CRU	Observed	-	1901-2018	0.5° × 0.5° (Harris et al., 2020)
GridMET ⁺	Observed	-	1950 - 2020	0.04° × 0.04° (Abatzoglou, 2013)
NASPA	Proxy + Downscaled	-	850* - 2016	0.5° × 0.5° (Stahle et al., 2020)
MIROC-ES2L	GCM	Past1000	850-1849	2.8° × 2.8° (Hajima et al., 2020)
MIROC-ES2L	GCM	Historical	1850- 2014	2.8° × 2.8° (Hajima et al., 2020)
MIROC-ES2L	GCM	SSP1-2.6 & SSP5-8.5	2015- 2100	2.8° × 2.8° (Hajima et al., 2020)
MRI-ESM2	GCM	Past1000	850 - 1849	100 km × 100 km (Yukimoto et al., 2019)
MRI-ESM2	GCM	Historical	1850 -2014	100 km × 100 km

MRI-ESM2	GCM	SSP1-2.6 & SSP5-8.5	2015- 2100	(Yukimoto et al., 2019) 100 km × 100 km (Yukimoto et al., 2019)
----------	-----	------------------------	------------	---

92 *NASPA starting year varies from 0-1400 C.E., depending on the grid location. This study used data from 850 C.E.
93 if it were available.

94 [†]US only

95

96 Spatial resolution followed NASPA grid placement and resolution ($0.5^\circ \times 0.5^\circ$) with relevant
97 time series from the other datasets selected based on the shortest distance to the NASPA grid
98 center. GridMET data is only available for the Continental United States, so was not included
99 outside this region.

100 2.2. Temporal Downscaling

101 Precipitation was considered at a monthly resolution, natively for all datasets except for the bi-
102 annual NASPA, which was temporally downsampled following the approach of Sung and Stagge
103 (2022) using K-nearest neighbor (KNN) resampling (Gangopadhyay et al., 2005). Here, KNN
104 resampling was used to insert 13-month SPI-3 series from the observed record into a given
105 NASPA year based on similarity to the 3 bracketing NASPA estimates (prior year's MJJ,
106 concurrent DJFMA, and concurrent MJJ). Global Precipitation Climatology Centre (GPCC)
107 precipitation was used as the historical catalog because it was originally used for NASPA
108 calibration.

109 KNN resampling used SPI-3 sequences, then converted to precipitation, rather than precipitation
110 sequences. This increased the sampling catalog twelve-fold, avoiding repetition in resampling,
111 and was reasonable because normalized SPI-3 values are independent of season. Ten annual
112 historical SPI-3 sequences were resampled ($K=10$), converted back to precipitation, and then
113 averaged to produce the monthly NASPA estimate and associated uncertainty.

114 2.3. Non-Stationary SPI

115 A non-stationary SPI (NSPI) approach (Sung et al., 2022) was used to simultaneously model
116 centennial-scale trends of droughts and pluvials and to account for data-induced bias. The NSPI
117 is similar to the the SPI by fitting probability density functions to accumulated precipitation, but
118 allows distribution parameters to shift gradually through time (Pedersen et al., 2019; Wood,
119 2008). The two parameters of the gamma distribution (mean, μ and shape, α) were modeled
120 simultaneously by month and year to simultaneously capture recurring seasonality (monthly) and

121 multi-decadal trends (year) (Eqs. 1-3). Here, $P_{3-month,m,y}$ represents the 3-month average
 122 precipitation rate at month m and year y . This model therefore captures shifts in the underlying
 123 distribution, from which we can extract changes in drought and pluvials, defined as SPI= -1.5
 124 (percentile = 6.7%) and SPI = 1.5 (percentile = 93.3%), respectively.

125 To account for data bias in the mean (Eq 2) and shape (Eq 3) parameters, the model included a
 126 unique intercept, β_0 , and a spline function to account for seasonally differing biases, $\beta_1 f_s$. The
 127 function f_s is a cubic polynomial spline controlled by β at each control point. The final term,
 128 $f_{te}(X_{year}, X_{month})$, represents the common smoothed long-term trend and seasonality after
 129 accounting for biases, modeled as a tensor product spline function.

$$P_{3\text{ month},m,y} = \text{gamma}(\mu, \alpha) \begin{pmatrix} m: \text{month}, \\ y: \text{year} \end{pmatrix} \quad (1)$$

$$\mu = \beta_{0\mu} \begin{pmatrix} CRU \\ NASPA \\ Gridmet \\ MRI \\ MIROC \end{pmatrix} + \beta_{1\mu} f_{s,\mu} \begin{pmatrix} CRU \\ NASPA \\ Gridmet \\ MRI \\ MIROC \end{pmatrix} + \beta_{2\mu} f_{te,\mu}(X_{year}, X_{month}) \quad (2)$$

$$\frac{1}{\log(\alpha)} = \beta_{0\alpha} + \beta_{0\alpha} f_{s,\alpha} \begin{pmatrix} CRU \\ NASPA \\ Gridmet \\ MRI \\ MIROC \end{pmatrix} + \beta_{1\alpha} f_{s,\alpha} \begin{pmatrix} CRU \\ NASPA \\ Gridmet \\ MRI \\ MIROC \end{pmatrix} + \beta_{2\alpha} f_{te,\alpha}(X_{year}, X_{month}) \quad (3)$$

130

131 CRU precipitation was considered ‘ground truth’ for bias correction because it is a land-based
 132 observation dataset that has undergone validation. Biases are assumed stationary through time;
 133 thereby bias estimated during the overlapping period with CRU will remain constant over the
 134 entire record length. This bias correction approach is similar to quantile mapping (Lanzante et
 135 al., 2018), as the $f(X_{month}, by = model)$ terms adjust the distribution mean and shape parameters,
 136 with the added spline constraint that limits bias correction from changing dramatically month to
 137 month.

138 **2.4. Significance tests**

139 Significance testing was based on gamma distribution comparisons, always using 1840-1860 as
 140 the pre-Industrial climatology (IPCC, 2014). The null hypothesis assumed that current (2000-

141 2020) or future (2080-2100) precipitation values for $SPI = \pm 1.5$ were equivalent to pre-Industrial
142 values. 10,000 random samples of the mean and shape parameter were taken from the modeled
143 distributions of the pre-Industrial and comparison time period to capture parameter uncertainty
144 while accounting for covariance. The significance of shifts in the precipitation extremes was
145 determined by a two-tailed test in which the null hypothesis was rejected when more than 97.5%
146 of random samples agreed with the sign of precipitation difference. This method is conceptually
147 similar to a two-tailed paired t-test with $\alpha=0.05$ but uses random samples from modeled
148 distributions (Chow, 1960).

149 **3. Results**

150 **3.1. Anthropogenic Period (1850-2100 CE) Trends**

151 First, we examined modern changes in the 3-month drought and pluvial precipitation ($SPI =$
152 ± 1.5), by comparing current (2000-2020) and future (2080-2100) time slices from the NSPI
153 model to the recent pre-Industrial baseline (1840-1860) (Figs. 1 and 2). For most regions and
154 seasons, pluvial precipitation has increased (Fig. 2), while droughts have become drier (Fig. 1),
155 with these trends projected to worsen throughout the next century regardless of emissions
156 scenario. This pattern of intensifying both extremes, less precipitation during drought years and
157 more precipitation during pluvials, is especially apparent in the Central and Eastern US. Pluvial
158 intensification is most common during winter (NDJ) and spring (FMA) (Fig. 2), while drought
159 intensification is most spatially extensive during summer (MJJ) and fall (ASO) (Fig. 1).

160

161 Not all regions show intensification of both extremes, instead experiencing exclusively wetter or
162 drier trends. Mexico and the southwestern US have become drier for both drought and pluvial
163 extremes across most seasons, with the most consistently significant decreases during drought
164 years. Conversely, eastern Canada has/will become wetter at both extremes, most substantially
165 during cool seasons (NDJ and FMA), resulting in worsening pluvials, but lessening droughts.

166

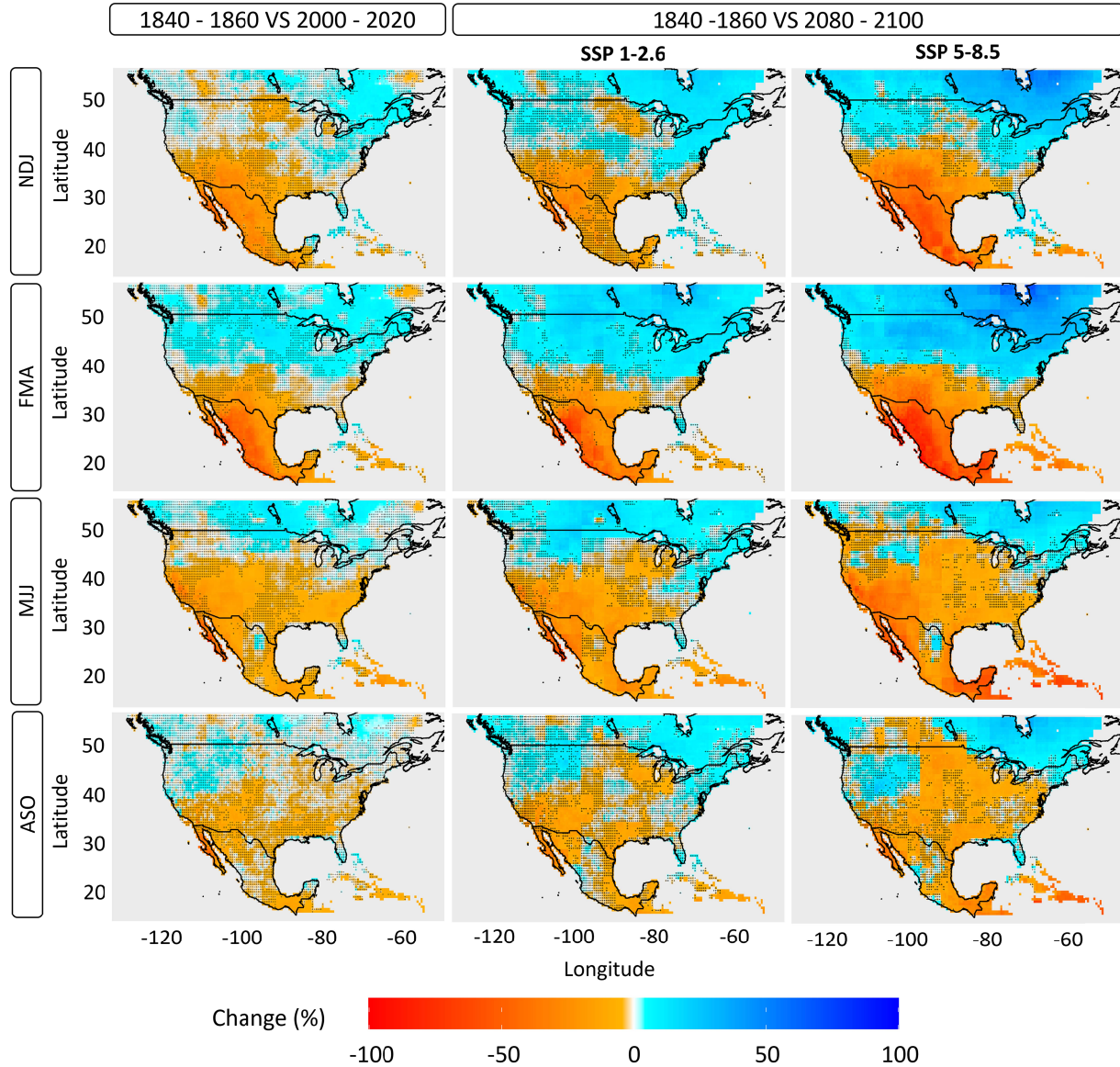
167 Pluvial and drought trends form spatially consistent regions despite all grid cells being modeled
168 independently. That is, trends do not change radically over short distances, but rather transition
169 smoothly in space. This lends further support to the findings, showing a strong spatiotemporal
170 signal that stands apart from random noise, despite independent calibration. The specific 3-

171 month periods displayed here were chosen to align with the NASPA seasons (MJJ, DJFMA)
172 (Stahle et al., 2020).

173

174 Cool season droughts follow a distinct latitudinal breakpoint, with lessening winter drought
175 above 40°N and worsening winter drought below 40°N (Fig. 1, top rows), reminiscent of
176 latitudinal gradients noted previously for the western US (Swain et al., 2018). Lessening winter
177 drought is most notable in Eastern Canada, where winter drought precipitation is projected to
178 increase by almost 50% for both future scenarios. Mexico and the southwestern US have already
179 experienced significant intensification of winter drought and is projected to worsen, reducing
180 precipitation amounts associated with a moderate/severe drought (SPI= -1.5) by almost 100%
181 relative to 1840-1860 climatology (Fig. 1). The trend towards lessening cool season drought
182 extremes is not statistically significant to date, but is projected to become significant by the end
183 of the century, whereas the trend towards worsening winter drought extremes across much of
184 southern North America has already shown significant changes relative to pre-Industrial
185 climatology.

186 During warm seasons (MJJ and ASO), the region of worsening drought expands to cover much
187 of North America (Fig. 1), but showing relatively smaller change. Mexico, the southwestern US,
188 and the Caribbean show especially significant warm season drought precipitation decreases. This
189 is particularly deleterious when considered alongside their significant cool season drought
190 intensification, leading to drought intensification throughout the year. Because these regions rely
191 on the warm season North American Monsoon (July -September) for a majority of their annual
192 precipitation (Grantz et al., 2007), intensified warm season drought increases risks of water
193 shortage by failing to refill reservoirs. Some exceptions to the worsening warm season drought
194 trend exist (northern intermountain western US and central Mexico plateau), which may be
195 related to the spatial complexity of mountainous precipitation (Preece et al., 2021).



196
 197 *Figure 1. Percent precipitation change compared to pre-Industrials for drought years (SPI = -1.5). (left): current era (center)*
 198 *future under ssp1-2.6, (right) ssp5-8.5 scenarios.*

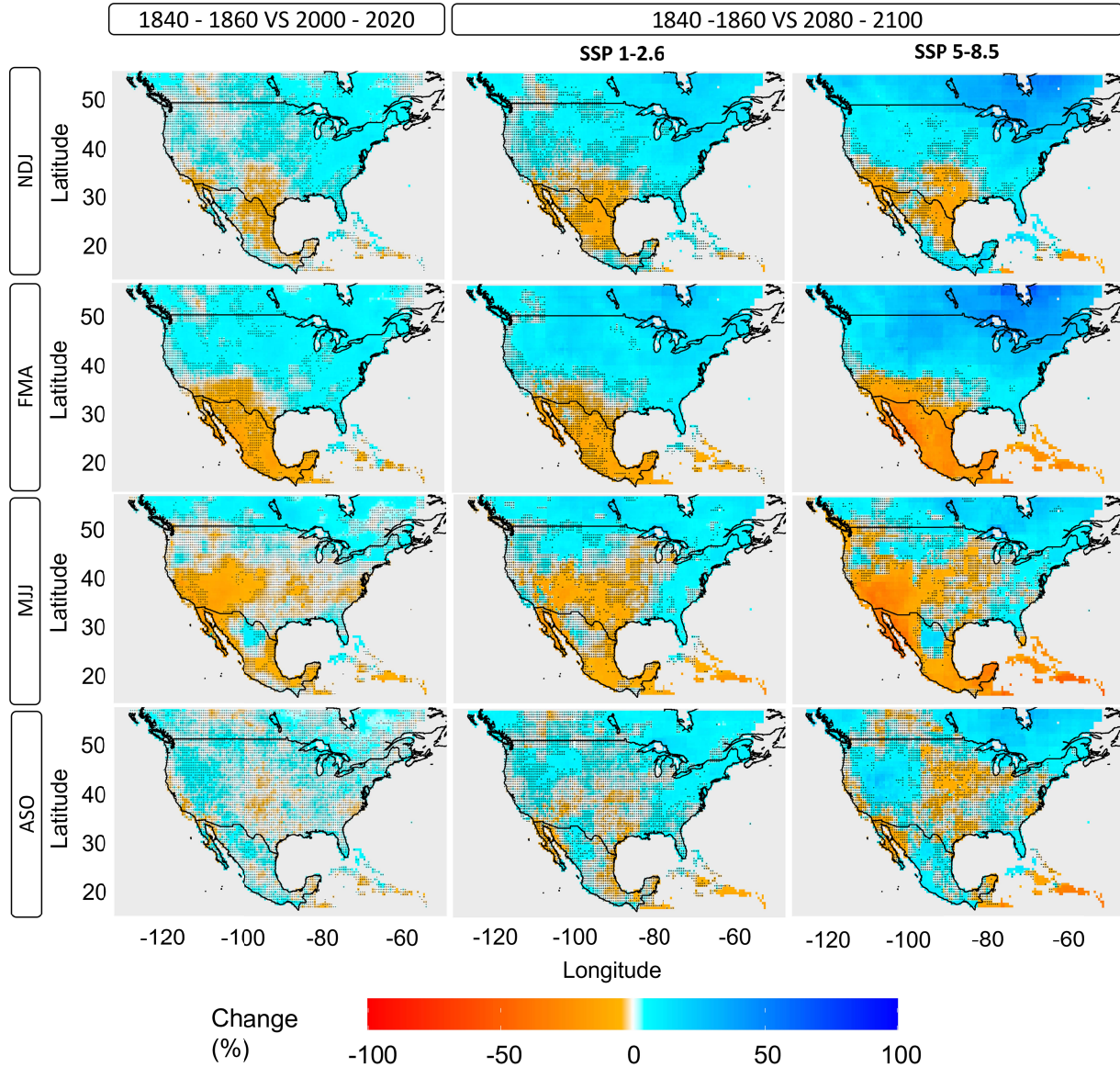
199 Pluvials have intensified for most of North America (Fig. 2), except for Mexico and the
 200 southwestern US, particularly during cool seasons. The intensification of cool season pluvials is
 201 most significant across eastern North America, with this region expanding to cover much of the
 202 US and Canada during future scenarios (Fig. 2, top rows). While trends in the eastern US and
 203 Canada are more spatially homogenous, we note that the strongest winter pluvial intensification
 204 in the west occurs in mountainous topography during the early spring (FMA).

205

206 During the MJJ early summer period, the region of decreasing wet extremes expands northward
207 centered on the southwestern US. With increasing CO₂ forcing, this trend intensifies in
208 magnitude and expands spatially to include the American Plains and the Caribbean. Our finding
209 of a decrease in MJJ pluvials followed by little change during ASO mirrors previous findings of
210 a seasonal delay in the North American Monsoon under climate change (B. I. Cook & Seager,
211 2013; Pascale et al., 2017; Prein et al., 2022).

212
213 For all locations, future scenarios are extensions of the last century with no notable sign changes
214 between 2020 and 2100. Trends for many regions are already statistically significant during the
215 instrumental period (1850-2020) and where they are not, trends often become significant under
216 one or both future climate change scenarios. This implies that climate change has begun to
217 affect precipitation in a manner consistent with GCM simulations under increased greenhouse gas
218 concentrations and is likely to become more intense and detectable through the 21st century.

219

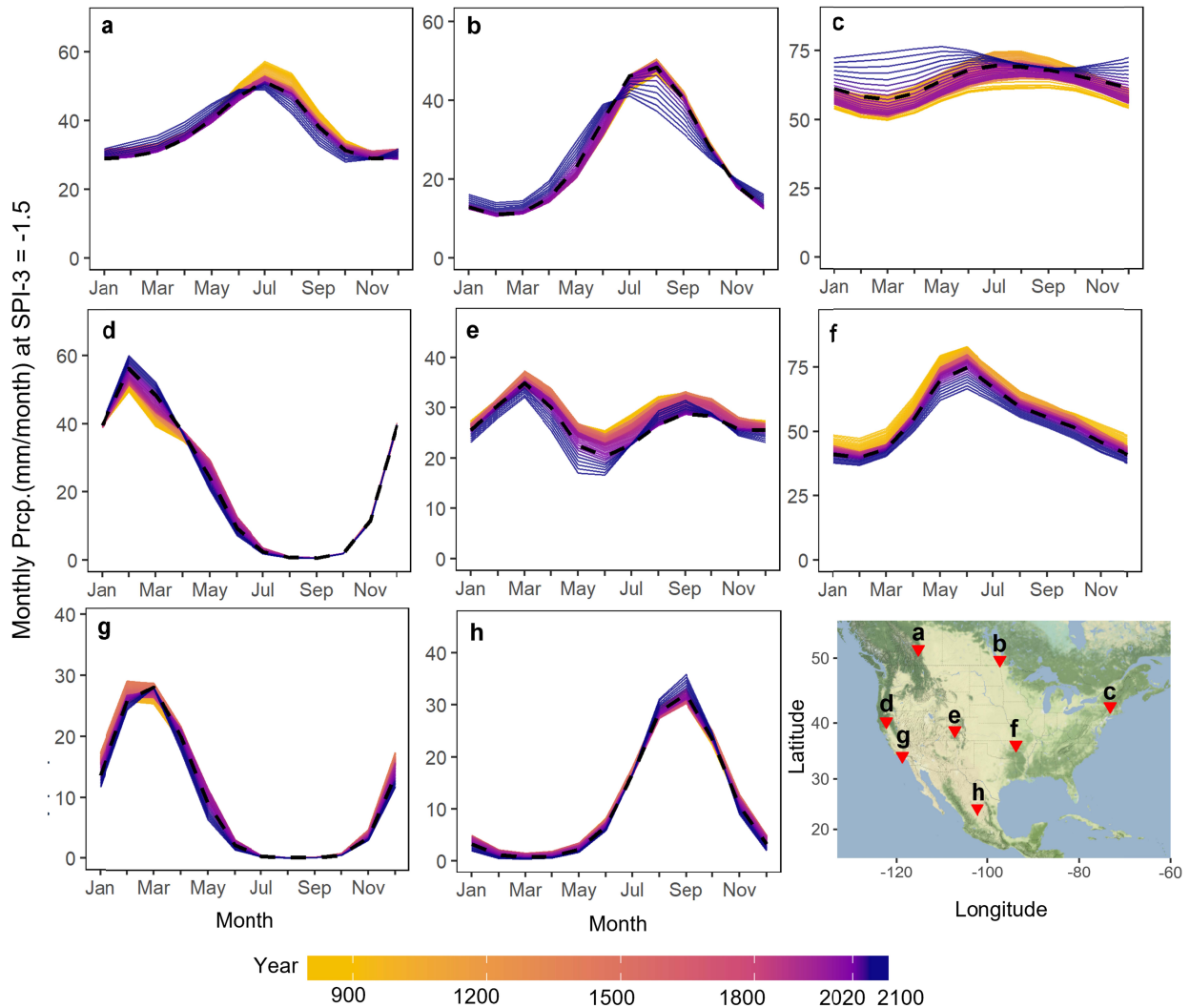


220
 221 *Figure 2. Percent precipitation changes compared to pre-Industrials for pluvial years (SPI = +1.5). (left) current era (center)*
 222 *future under ssp1-2.6, (right) ssp5-8.5 scenarios.*

223 **3.2. Millenium-Scale (850-2100 CE) Context**

224
 225 The ability to consider non-linear precipitation patterns in a longer context of natural climate
 226 variability using the full 1,250-year model is a major benefit of our approach. Using identical
 227 drought and pluvial definitions for several representative locations (Fig. 3, 4, S1 and S2), we find
 228 similar patterns: cool season wetting trends and warm season drying trends for northern locations

229 (Figs 3 and S1, top row), intensified pluvials and drought in mid-latitude region between 30°- 40°
 230 latitude (mid row), and severe drying trends in the south (bottom row).



231
 232 *Figure 3. Seasonal precipitation in long-term trends at SPI = -1.5 for a single grid cell. Panels are organized spatially, with*
 233 *labels corresponding to the map in the bottom right. x-axis: the final month of the SPI-3 period (i.e., May :Mar-May precipitation*
 234 *rates). All future changes are modeled using the SSP 5-8.5 scenario.*

235 For the three northern reference sites (Figs. 3 and S1, a-c) shows weakened seasonality as overall
 236 precipitation during the winter dry season (Jan - Apr) becomes wetter, while the summer wet
 237 season (Jul - Sep) becomes drier. These phenomena are also captured in Figs S2 and S3. Unlike the
 238 northern sites, the two mid-latitude reference sites in the center of the continent (Figs. 3e and 3f)
 239 exhibit wetter pluvials and drier droughts for all seasons. This greatly increases the interannual
 240 variability for the region, fluctuating between increasingly wider extremes. Despite some natural

241 pre-Industrial fluctuation, the most extreme shifts for all of these sites occur after 1850, further
242 emphasizing that modern and projected precipitation shifts are outside pre-Industrial (850-1850
243 CE) natural variability, as tested in Figs. 1 and 2.

244

245 The southern-most reference site, Mexico City (Fig. 3h), exhibits a shift towards drier conditions
246 for both drought and pluvial years across most seasons, with the most dramatic changes
247 occurring during the wet season (Jul-Sep). In future projections under high emissions scenarios,
248 drought year precipitation is nearly 50% of the pre-Industrial, with decreases already emerging in
249 the present (2020).

250

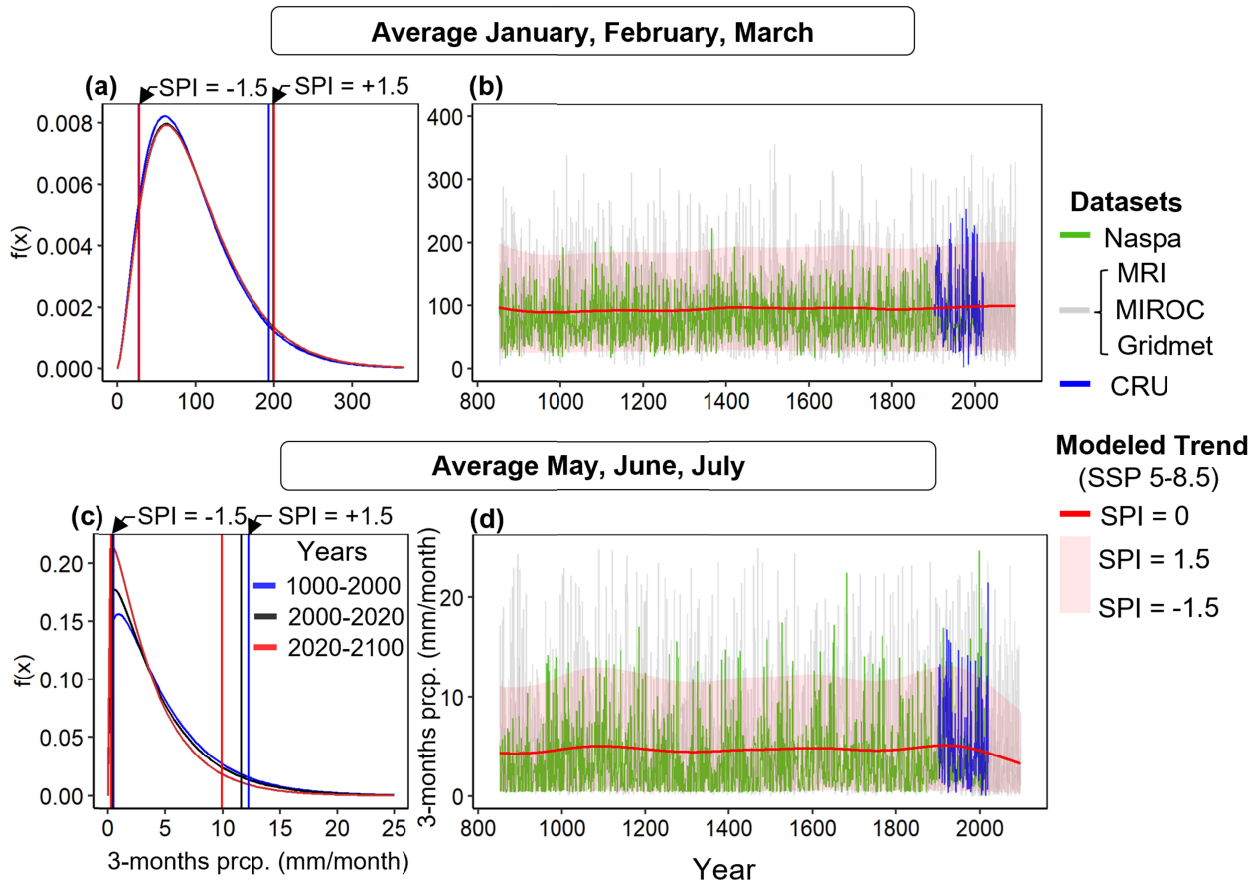
251 Northern and southern California, shown to the far left (Figs. 3d and g), both exhibit modern
252 (post 1850) decrease in spring and early summer precipitation, with this trend particularly intense
253 in Southern California. Modern drought decreases in Southern California continue throughout
254 the summer and into the fall, whereas no equivalent trends exist in northern California (Fig 1).
255 Finally, both northern and southern California have experienced a long trend towards increased
256 pluvial year precipitation during the wet winter season beginning well before the Industrial
257 period (ca 1100 CE) (Figs 3 and 4). To better illustrate centennial-scale shifts in southern
258 California precipitation, we examine the wet season pluvial increase (JFM), and the notable
259 drying of the summer shoulder season (MJJ) (Fig 4).

260

261 JFM pluvial increases run counter to the overwhelming drying trend in southern California and
262 the surrounding region, as indicated by a rightward shift in the distribution's upper tail and an
263 increase in the upper bound through time (Fig 4a). This winter pluvial wetting trend occurred
264 gradually over the last millennium, since 1000 CE, with no detectable acceleration during the
265 Industrial period or into the future. The cool season in southern California is where NASPA has
266 the best cross-validation skill (Stahle et al., 2020), lending confidence to these findings. Others
267 have simulated relatively little change in extremely wet seasons during the 1900s and increases
268 by 2100 (Swain et al., 2018), though our findings suggest this trend may be part of a gradual
269 pluvial increase beginning centuries prior. It should be noted that the gradual precipitation
270 increase for JFM pluvials is not reflected during drought years, which instead show a

271 precipitation decrease, widening the gap between wet and dry years during the critical winter
 272 precipitation period.

273



274

275 *Figure 4. Modeled precipitation changes at Los Angeles, CA, USA. (Left) Fitted Gamma distributions for different periods with*
 276 *drought and pluvial thresholds. (Right) time series of underlying data, the bias-corrected mean, drought and pluvial thresholds.*

277 A severe decrease in southern California precipitation occurs during the early summer MJJ
 278 season (Figs 3g and 4c), with modern climatology (black) slightly drier than pre-Industrial
 279 conditions (blue), whereas future extremes (red) indicate rapidly decreasing precipitation. While
 280 the model does not explicitly consider zero precipitation years, a detectable shift towards the
 281 zero bound suggests an increase in the frequency of years with zero precipitation during the MJJ
 282 season. Large decreases also occur in the upper tail, indicating less early summer precipitation
 283 even during particularly wet years. This decreasing trend is sudden and stands out from the prior
 284 thousand years of natural climate variability (Fig. 4d), suggesting an anthropogenic cause.

285

286 Considered together, southern California has experienced a gradual increase in wet season
287 pluvials and a sudden 20th century decrease in spring and early summer precipitation, which
288 generally agrees with prior studies indicating intensifying seasonality and extremes (Persad et al.,
289 2020; Swain et al., 2018; Williams et al., 2022). This intensification complicates regional water
290 management already experiencing a decade long drought (Diffenbaugh et al., 2015; Williams et
291 al., 2020). Precipitation decreases during the spring and early summer lengthens the duration of
292 the summer dry season, increasing reliance on reservoir storage accumulated during the wet
293 period from three distinct source areas: northern California's Sierra Nevada mountains, the
294 Colorado River, and locally (Pagán et al., 2016; Woodhouse et al., 2020). Increasing annual
295 variability make Sierra Nevada and local sources more uncertain (Fig. 3d and g), whereas the
296 Colorado River Basin is projected to undergo dramatic decreases over the next century (Fig. 1
297 and 2), further exacerbating water management risks.

298

299 **4. Discussions and Conclusions**

300

301 The approach used here, integrating datasets from the past through the future, relies on a novel
302 use of hierarchical spline models (Sung et al., 2022) to provide a comprehensive view of modern
303 and projected drought and pluvial extremes in the context of centuries of pre-industrial climate.
304 By considering overlapping data types, distribution shifts only become significant when
305 consistent across multiple sources and decades. Thus, GCM simulations support NASPA
306 reconstruction skill gaps, like the northeast cool season or the ASO interpolated season (Stahle et
307 al., 2020), while integrative splines improved parameter stability. Spatial agreement across
308 thousands of independently modeled cells provides further confidence in these findings.

309

310 Our results highlight many regions which experienced sharp hydroclimate trends during the 20th
311 and 21st centuries relative to a largely stable precipitation climatology during the prior 1,000
312 years. Drier summer droughts and wetter winter pluvials are typical across much of North
313 America, particularly in the east and north. Unlike these regions with wider interannual
314 variability, the south and southwest show consistent drying trends, while the far northeast and
315 eastern Canada exhibit consistent wetting trends. Our findings agree with prior studies
316 suggesting that climate change has intensified the hydrologic cycle, worsening drought risks

317 during historical dry seasons (Chou et al., 2013; Dai, 2013; Diffenbaugh et al., 2015; Lehner et
318 al., 2018) and increasing pluvial magnitudes during wet seasons for many regions (Diffenbaugh
319 & Davenport, 2021; Swain et al., 2018) with projected future intensification. Increases in
320 interannual variability for mid-latitude regions and rapid trends toward dryer[wetter] conditions
321 in the south[north] with more intense extremes makes water management more challenging as
322 infrastructure and strategies developed in the early or mid-1900s using that time’s climatology is
323 often no longer representative of current or future climate extremes (Gangopadhyay et al., 2022;
324 Mallakpour et al., 2019). We expect our study contributes to water infrastructure adaptation to a
325 “new climate normal” (Hoylman et al., 2022) through improved quantification of hydroclimatic
326 trends placed into a millennial-scale context.

327

328 **Acknowledgments**

329 This work was supported by the National Science Foundation Project No. 2002539, Byrd Polar
330 and Climate Research Center, and the Ohio Supercomputer Center.

331 **Open Research**

332 NASPA data is available at

333 <https://www.ncei.noaa.gov/pub/data/paleo/treering/reconstructions/northamerica/NASPA/>.

334 CRU and GridMET datasets are available at

335 <https://crudata.uea.ac.uk/cru/data/hrg/index.htm#current> and

336 <https://www.climatologylab.org/gridmet.html>, respectively.

337 GCM datasets (MIROC-ES2L and MRI-ESM2) can be downloaded from <https://esgf->

338 node.llnl.gov/search/cmip6/.

339 The Non-stationary SPI modeling used ‘mgcv’ packages(Wood, 2008) in R. All code is

340 preserved at <https://doi.org/10.5281/zenodo.7789830>.

341

342

343

344

345

346

347 **References**

- 348 Abatzoglou, J. T. (2013). Development of gridded surface meteorological data for ecological applications and
349 modelling. *International Journal of Climatology*, 33(1), 121–131. <https://doi.org/10.1002/joc.3413>
- 350 Ault, T. R. (2020). On the essentials of drought in a changing climate. *Science*, 368(6488), 256–260.
351 <https://doi.org/10.1126/science.aaz5492>
- 352 Bishop, D. A., Williams, A. P., Seager, R., Cook, E. R., Peteet, D. M., Cook, B. I., et al. (2021). Placing the east-
353 west North American aridity gradient in a multi-century context. *Environmental Research Letters*, 16(11),
354 114043. <https://doi.org/10.1088/1748-9326/ac2f63>
- 355 Chou, C., Chiang, J. C. H., Lan, C.-W., Chung, C.-H., Liao, Y.-C., & Lee, C.-J. (2013). Increase in the range
356 between wet and dry season precipitation. *Nature Geoscience*, 6(4), 263–267.
357 <https://doi.org/10.1038/ngeo1744>
- 358 Chow, G. C. (1960). Tests of Equality Between Sets of Coefficients in Two Linear Regressions. *Econometrica*,
359 28(3), 591–605. <https://doi.org/10.2307/1910133>
- 360 Cook, B., Seager, R., Williams, A. P., Puma, M. J., McDermid, S., Kelley, M., & Nazarenko, L. (2019). Climate
361 Change Amplification of Natural Drought Variability: The Historic Mid-Twentieth-Century North
362 American Drought in a Warmer World. *Journal of Climate*, 32(17), 5417–5436.
363 <https://doi.org/10.1175/JCLI-D-18-0832.1>
- 364 Cook, B. I., & Seager, R. (2013). The response of the North American Monsoon to increased greenhouse gas
365 forcing. *Journal of Geophysical Research: Atmospheres*, 118(4), 1690–1699.
366 <https://doi.org/10.1002/jgrd.50111>
- 367 Cui, T., Li, C., & Tian, F. (2021). Evaluation of Temperature and Precipitation Simulations in CMIP6 Models Over
368 the Tibetan Plateau. *Earth and Space Science*, 8(7), e2020EA001620.
369 <https://doi.org/10.1029/2020EA001620>
- 370 Dai, A. (2013). Increasing drought under global warming in observations and models. *Nature Climate Change*, 3(1),
371 52–58. <https://doi.org/10.1038/nclimate1633>

- 372 Diffenbaugh, N. S., & Davenport, F. V. (2021). On the impossibility of extreme event thresholds in the absence of
373 global warming. *Environmental Research Letters*, *16*(11), 115014. [https://doi.org/10.1088/1748-](https://doi.org/10.1088/1748-9326/ac2f1a)
374 [9326/ac2f1a](https://doi.org/10.1088/1748-9326/ac2f1a)
- 375 Diffenbaugh, N. S., Swain, D. L., & Touma, D. (2015). Anthropogenic warming has increased drought risk in
376 California. *Proceedings of the National Academy of Sciences*, *112*(13), 3931–3936.
377 <https://doi.org/10.1073/pnas.1422385112>
- 378 Diffenbaugh, N. S., Singh, D., Mankin, J. S., Horton, D. E., Swain, D. L., Touma, D., et al. (2017). Quantifying the
379 influence of global warming on unprecedented extreme climate events. *Proceedings of the National*
380 *Academy of Sciences*, *114*(19), 4881–4886. <https://doi.org/10.1073/pnas.1618082114>
- 381 Eyring, V., Bony, S., Meehl, G. A., Senior, C. A., Stevens, B., Stouffer, R. J., & Taylor, K. E. (2016). Overview of
382 the Coupled Model Intercomparison Project Phase 6 (CMIP6) experimental design and organization.
383 *Geoscientific Model Development*, *9*(5), 1937–1958. <https://doi.org/10.5194/gmd-9-1937-2016>
- 384 Gangopadhyay, S., Clark, M., & Rajagopalan, B. (2005). Statistical downscaling using K-nearest neighbors. *Water*
385 *Resources Research*, *41*(2). <https://doi.org/10.1029/2004WR003444>
- 386 Gangopadhyay, S., Woodhouse, C. A., McCabe, G. J., Routson, C. C., & Meko, D. M. (2022). Tree Rings Reveal
387 Unmatched 2nd Century Drought in the Colorado River Basin. *Geophysical Research Letters*, *49*(11),
388 e2022GL098781. <https://doi.org/10.1029/2022GL098781>
- 389 Grantz, K., Rajagopalan, B., Clark, M., & Zagana, E. (2007). Seasonal Shifts in the North American Monsoon.
390 *Journal of Climate*, *20*(9), 1923–1935. <https://doi.org/10.1175/JCLI4091.1>
- 391 Hajima, T., Watanabe, M., Yamamoto, A., Tatebe, H., Noguchi, M. A., Abe, M., et al. (2020). Development of the
392 MIROC-ES2L Earth system model and the evaluation of biogeochemical processes and feedbacks.
393 *Geoscientific Model Development*, *13*(5), 2197–2244. <https://doi.org/10.5194/gmd-13-2197-2020>
- 394 Harris, I., Osborn, T. J., Jones, P., & Lister, D. (2020). Version 4 of the CRU TS monthly high-resolution gridded
395 multivariate climate dataset. *Scientific Data*, *7*(1), 109. <https://doi.org/10.1038/s41597-020-0453-3>
- 396 Heim, R. R. (2002). A Review of Twentieth-Century Drought Indices Used in the United States. *Bulletin of the*
397 *American Meteorological Society*, *83*(8), 1149–1166. <https://doi.org/10.1175/1520-0477-83.8.1149>
- 398 Ho, M., Lall, U., Allaire, M., Devineni, N., Kwon, H. H., Pal, I., et al. (2017). The future role of dams in the United
399 States of America. *Water Resources Research*, *53*(2), 982–998. <https://doi.org/10.1002/2016WR019905>

- 400 Hoylman, Z. H., Bocinsky, R. K., & Jencso, K. G. (2022). Drought assessment has been outpaced by climate
401 change: empirical arguments for a paradigm shift. *Nature Communications*, *13*(1), 2715.
402 <https://doi.org/10.1038/s41467-022-30316-5>
- 403 IPCC. (2014). *Climate Change 2013: The Physical Science Basis: Working Group I Contribution to the Fifth*
404 *Assessment Report of the Intergovernmental Panel on Climate Change*. Cambridge University Press.
- 405 Lanzante, J. R., Dixon, K. W., Nath, M. J., Whitlock, C. E., & Adams-Smith, D. (2018). Some Pitfalls in Statistical
406 Downscaling of Future Climate. *Bulletin of the American Meteorological Society*, *99*(4), 791–803.
407 <https://doi.org/10.1175/BAMS-D-17-0046.1>
- 408 Lehner, F., Coats, S., Stocker, T. F., Pendergrass, A. G., Sanderson, B. M., Raible, C. C., & Smerdon, J. E. (2017).
409 Projected drought risk in 1.5°C and 2°C warmer climates. *Geophysical Research Letters*, *44*(14), 7419–
410 7428. <https://doi.org/10.1002/2017GL074117>
- 411 Lehner, F., Deser, C., Simpson, I. R., & Terray, L. (2018). Attributing the U.S. Southwest’s Recent Shift Into Drier
412 Conditions. *Geophysical Research Letters*, *45*(12), 6251–6261. <https://doi.org/10.1029/2018GL078312>
- 413 Mallakpour, I., AghaKouchak, A., & Sadegh, M. (2019). Climate-Induced Changes in the Risk of Hydrological
414 Failure of Major Dams in California. *Geophysical Research Letters*, *46*(4), 2130–2139.
415 <https://doi.org/10.1029/2018GL081888>
- 416 Marvel, K., Cook, B. I., Bonfils, C., Smerdon, J. E., Williams, A. P., & Liu, H. (2021). Projected Changes to
417 Hydroclimate Seasonality in the Continental United States. *Earth’s Future*, *9*(9), e2021EF002019.
418 <https://doi.org/10.1029/2021EF002019>
- 419 Pagán, B. R., Ashfaq, M., Rastogi, D., Kendall, D. R., Kao, S.-C., Naz, B. S., et al. (2016). Extreme hydrological
420 changes in the southwestern US drive reductions in water supply to Southern California by mid century.
421 *Environmental Research Letters*, *11*(9), 094026. <https://doi.org/10.1088/1748-9326/11/9/094026>
- 422 Pascale, S., Boos, W. R., Bordoni, S., Delworth, T. L., Kapnick, S. B., Murakami, H., et al. (2017). Weakening of
423 the North American monsoon with global warming. *Nature Climate Change*, *7*(11), 806–812.
424 <https://doi.org/10.1038/nclimate3412>
- 425 Pedersen, E. J., Miller, D. L., Simpson, G. L., & Ross, N. (2019). Hierarchical generalized additive models in
426 ecology: an introduction with mgcv. *PeerJ*, *7*, e6876. <https://doi.org/10.7717/peerj.6876>

- 427 Persad, G. G., Swain, D. L., Kouba, C., & Ortiz-Partida, J. P. (2020). Inter-model agreement on projected shifts in
428 California hydroclimate characteristics critical to water management. *Climatic Change*, *162*(3), 1493–1513.
429 <https://doi.org/10.1007/s10584-020-02882-4>
- 430 Preece, J. R., Shinker, J. J., Riebe, C. S., & Minckley, T. A. (2021). Elevation-dependent precipitation response to El
431 Niño-Southern oscillation revealed in headwater basins of the US central Rocky Mountains. *International
432 Journal of Climatology*, *41*(2), 1199–1210. <https://doi.org/10.1002/joc.6790>
- 433 Prein, A. F., Towler, E., Ge, M., Llewellyn, D., Baker, S., Tighi, S., & Barrett, L. (2022). Sub-Seasonal
434 Predictability of North American Monsoon Precipitation. *Geophysical Research Letters*, *49*(9),
435 e2021GL095602. <https://doi.org/10.1029/2021GL095602>
- 436 Stagge, J. H., & Sung, K. (2022). A Non-stationary Standardized Precipitation Index (NSPI) using Bayesian Splines.
437 *Journal of Applied Meteorology and Climatology*, *1*(aop). <https://doi.org/10.1175/JAMC-D-21-0244.1>
- 438 Stahle, D. W., Cook, E. R., Burnette, D. J., Torbenson, M. C. A., Howard, I. M., Griffin, D., et al. (2020).
439 Dynamics, Variability, and Change in Seasonal Precipitation Reconstructions for North America. *Journal
440 of Climate*, *33*(8), 3173–3195. <https://doi.org/10.1175/JCLI-D-19-0270.1>
- 441 Stevenson, S., Coats, S., Touma, D., Cole, J., Lehner, F., Fasullo, J., & Otto-Bliesner, B. (2022). Twenty-first
442 century hydroclimate: A continually changing baseline, with more frequent extremes. *Proceedings of the
443 National Academy of Sciences*, *119*(12), e2108124119. <https://doi.org/10.1073/pnas.2108124119>
- 444 Sung, K., Torbenson, M. C. A., & Stagge, J. H. (2022). Assessing decadal to centennial scale nonstationary
445 variability in meteorological drought trends. *Hydrology and Earth System Sciences, EGU sphere*.
446 <https://doi.org/10.5194/egusphere-2022-476>
- 447 Swain, D. L., Langenbrunner, B., Neelin, J. D., & Hall, A. (2018). Increasing precipitation volatility in twenty-first-
448 century California. *Nature Climate Change*, *8*(5), 427–433. <https://doi.org/10.1038/s41558-018-0140-y>
- 449 Williams, A. P., Cook, E. R., Smerdon, J. E., Cook, B. I., Abatzoglou, J. T., Bolles, K., et al. (2020). Large
450 contribution from anthropogenic warming to an emerging North American megadrought. *Science*,
451 *368*(6488), 314–318. <https://doi.org/10.1126/science.aaz9600>
- 452 Williams, A. P., Cook, B. I., & Smerdon, J. E. (2022). Rapid intensification of the emerging southwestern North
453 American megadrought in 2020–2021. *Nature Climate Change*, *12*(3), 232–234.
454 <https://doi.org/10.1038/s41558-022-01290-z>

455 Wood, S. N. (2008). Fast stable direct fitting and smoothness selection for generalized additive models. *Journal of*
456 *the Royal Statistical Society: Series B (Statistical Methodology)*, 70(3), 495–518.

457 <https://doi.org/10.1111/j.1467-9868.2007.00646.x>

458 Woodhouse, C. a., Meko, D. m., & Bigio, E. r. (2020). A Long View of Southern California Water Supply: Perfect
459 Droughts Revisited. *JAWRA Journal of the American Water Resources Association*, 56(2), 212–229.

460 <https://doi.org/10.1111/1752-1688.12822>

461 Yukimoto, S., Kawai, H., Koshiro, T., Oshima, N., Yoshida, K., Urakawa, S., et al. (2019). The Meteorological
462 Research Institute Earth System Model Version 2.0, MRI-ESM2.0: Description and Basic Evaluation of the
463 Physical Component. *Journal of the Meteorological Society of Japan. Ser. II, advpub*, 2019–051.

464 <https://doi.org/10.2151/jmsj.2019-051>

465